Bioorganic Chemistry 142 (2024) 106967

Contents lists available at ScienceDirect

Bioorganic Chemistry

journal homepage: www.elsevier.com/locate/bioorg

A new fluorescent probe for the visualization of progerin

Jon Macicior [1], Daniel Fernández [1], Silvia Ortega-Gutiérrez [*]

Departamento de Química Orgánica, Facultad de Ciencias Químicas, Plaza de las Ciencias s/n, Universidad Complutense de Madrid, E-28040 Madrid, Spain

ARTICLE INFO

Keywords:
Rare diseases
Progeria
HGPS
Aging
Senescence
Fluorescent probes
Progerin
Decursinol

ABSTRACT

Hutchinson-Gilford progeria syndrome (HGPS) or progeria is a rare genetic disease that causes premature aging, leading to a drastic reduction in the life expectancy of patients. Progeria is mainly caused by the intracellular accumulation of a defective protein called progerin, generated from a mutation in the LMNA gene. Currently, there is only one approved drug for the treatment of progeria, which has limited efficacy. It is believed that progerin levels are the most important biomarker related to the severity of the disease. However, there is a lack of effective tools to directly visualize progerin in the native cellular models, since the commercially available antibodies are not well suited for the direct visualization of progerin in cells from the mouse model of the disease. In this context, an alternative option for the visualization of a protein relies on the use of fluorescent chemical probes, molecules with affinity and specificity towards a protein. In this work we report the synthesis and characterization of a new fluorescent probe (UCM-23079) that allows for the direct visualization of progerin in cells from the most widely used progeroid mouse model. Thus, UCM-23079 is a new tool compound that could help prioritize potential preclinical therapies towards the final goal of finding a definitive cure for progeria.

1. Introduction

Hutchinson-Gilford progeria syndrome (HGPS) or progeria is a rare pediatric disease caused by a silent mutation (c.1824C > T) in exon 11 of the LMNA gene. This mutation activates a specific cryptic donor splice site in the lamin A transcript that generates an altered mRNA which, upon translation, generates a lamin A variant called progerin, characterized by a 50 amino acid deletion in its primary sequence and the presence of a permanently farnesylated and methylated C-terminal cysteine [1,2]. The presence of the farnesyl and methyl groups, absent in normal lamin A, increases progerin hydrophobicity and favors its abnormal accumulation in the nuclear envelope, leading to an altered nuclear morphology and an impaired functionality. These deficiencies give rise to numerous global cell defects that are eventually responsible for the complex and distinctive disease phenotype, characterized by an overall aged aspect of diseased children, who suffer from growth impairment, low body weight, absence of subcutaneous fat, lipodystrophy, decreased joint mobility, alopecia, and cardiovascular disease, being this latter pathology the main cause of death at the early age of 14–15 years on average [3]. Despite being a rare disease, progeria shares important similarities with physiological senescence and can be accordingly considered as an accelerated aging mode. This fact has stimulated research efforts aimed at finding a cure for the disease with the hope of not only being useful for progeria patients but also for providing valuable insights about the druggability of the aging process itself, one of the hottest topics of current research [4,5].

With the aim of developing new therapeutic strategies for the treatment of progeria, different approaches have been explored. These include targeting the enzymes involved in the post-translational processing of progerin such as farnesyl transferase (FTase) and isoprenylcysteine carboxylmethyltransferase (ICMT) or interfering with protein–protein interactions in which progerin is involved [6–10]. Also, biological therapies based on CRISPR/Cas9 system, antisense oligonucleotides or gene therapy approaches have been described [11–15]. Up to date, all these efforts have translated into the approval, in 2020, of the FTase inhibitor lonafarnib, which remains the only available treatment for progeria [16]. Although this approval has represented a major advance in the field, the improvement induced by this drug remains limited [17], fact that highlights the need for new therapeutic alternatives. One of the challenges hindering the advancement of new

Abbreviations: CETSA, cellular thermal shift assay; DDQ, 2,3-dichloro-5,6-dicyano-*p*-benzoquinone; FTase, farnesyl transferase; HGPS, Hutchinson-Gilford progeria syndrome; ICMT, isoprenylcysteine carboxylmethyltransferase; MW, microwave; PBS, phosphate buffered saline solution.

* Corresponding author.
E-mail address: siortega@ucm.es (S. Ortega-Gutiérrez).

[1] These authors contributed equally.

https://doi.org/10.1016/j.bioorg.2023.106967
Received 25 September 2023; Received in revised form 9 November 2023; Accepted 10 November 2023
Available online 11 November 2023

pharmacological approaches is the limited ability to visually assess progerin levels and localization within mouse progeroid cells. This limitation arises from the lack of commercially available antibodies that are able to detect progerin in mouse cells. Since the levels of progerin seem to be the most single important factor in the outcome of progeria, its direct visualization is key as a biomarker to inform about the efficacy of a potential treatment in the mouse model. In the absence of appropriate antibodies, chemical probes -fluorophore-bearing small molecules with affinity, specificity and selectivity towards a protein- represent one of the main alternatives to antibodies for protein visualization in native cellular systems [18–26]. In this work we report the design, synthesis and biological validation of a fluorescent probe, compound UCM-23079 (**1**), which enables the direct visualization of progerin in mouse cells using fluorescence microscopy, a technique for which commercially available antibodies against progerin are not well suited. Accordingly, UCM-23079 represents a new addition to the current arsenal of available tools for the study of progerin and should aid in the early validation of new therapeutic approaches, thus contributing to facilitate the translation of basic research findings and increasing the chances of success of ensuing clinical phases.

2. Results and discussion

2.1. Design and synthesis of chemical probe 1

Chemical probes consist of three parts: (i) a bioactive subunit, responsible for the recognition and effective binding to the target protein; (ii) a fluorophore, responsible for the visualization of the target protein, being preferable molecules with high absorption wavelengths to limit damage to biological samples; and (iii) a linker, responsible for separating these two moieties in order to avoid possible interactions that could decrease affinity. As the bioactive subunit, we selected (+)-decursinol, the structural scaffold present in the few progerin ligands described so far (Fig. 1) [9,10]. Regarding the fluorophore, we have selected sulfo-Cy5-azide, a commonly used fluorophore due to its high wavelength absorption (648 nm), which minimizes excessive damage to biological samples [27]. Likewise, previous studies carried out on (+)-decursinol derivatives suggested that the introduction of a (*E*)-3-phenylpropene moiety in position 7 of (+)-decursinol was well tolerated [9,10]. Hence, we selected *p*-hydroxycinnamic acid group as the linker, since it could be readily alkylated with a terminal alkyne that would enable the subsequent introduction of the azide bearing fluorophore using click chemistry. These considerations led to the design of compound **1** (Fig. 1) as a chemical probe for the visualization of progerin.

Although two routes for the synthesis of (+)-decursinol have been described, they are either rather long (around 56 h of reaction time) [28] or not very efficient (overall yield <7 %) [29]. Hence, we optimized several steps to obtain (+)-decursinol in a total time of less than 24 h keeping the best overall yield previously described [28] by using, whenever possible, flow chemistry and microwave (MW) irradiation. Thus, the synthetic route started with the continuous flow hydrogenation of commercially available 7-hydroxycoumarin or umbelliferone (Scheme 1) followed by reaction, under MW conditions, with 3-methyl-2-butenal in the presence of phenylboronic and propionic acids. These reagents promoted the formation of the quinone methide intermediate, which evolved to form the desired tricyclic lactone **3** whose oxidation with 2,3-dichloro-5,6-dicyano-*p*-benzoquinone (DDQ) under MW conditions yielded xanthyletin **4** in significant less time (6 h vs 54 h of total reaction time) and with a slightly better overall yield (58 %) than the one previously described (54 %) [28]. Then, regio- and enantioselective Jacobsen epoxidation of xanthyletin, followed by the stereospecific opening of the epoxide ring in the presence of sodium borohydride allowed to obtain (+)-decursinol (**6**).

With respect to the linker, it was prepared by Williamson reaction between methyl (*E*)-3-(4-hydroxyphenyl)acrylate and propargyl bromide (Scheme 1). Hydrolysis of the methyl ester and condensation of the resulting carboxylic acid **8** with (+)-decursinol in the presence of *N,N'*-dicyclohexylcarbodiimide (DCC) and catalytic amounts of 4-(dimethylamino)pyridine (DMAP) gave intermediate alkyne **9**, whose copper(I)-catalyzed cycloaddition reaction with sulfo-Cy5-azide, using conditions previously set up in our research group [30], afforded target compound **1** in good yield (Scheme 1).

2.2. Spectroscopic characterization and target engagement confirmation

To confirm the suitability of probe **1** for its use in confocal microscopy, we carried out its spectroscopic characterization. Measurements were carried out in aqueous (phosphate buffered saline solution, PBS, at pH = 7.4) and organic (ethanol) solvents to assess that the probe retained the high fluorescence intensity of the sulfo-Cy5 fluorophore in aqueous (PBS) and in a more hydrophobic medium, trying to emulate the local membrane environment surrounding progerin. Excitation and emission spectra (Fig. 2) confirmed good emission intensity and wavelength values, appropriate for the desired application, with a wavelength for the maximal emission (λ_{em}) of 666 nm. This wavelength is well-suited for cellular visualization experiments and allows for the simultaneous use of a nuclear cell marker such as Hoechst 33342 (which can be excited at 405 nm and its emission observed at 440–480 nm) and, in the case of multiplexed experiments, with additional fluorophores

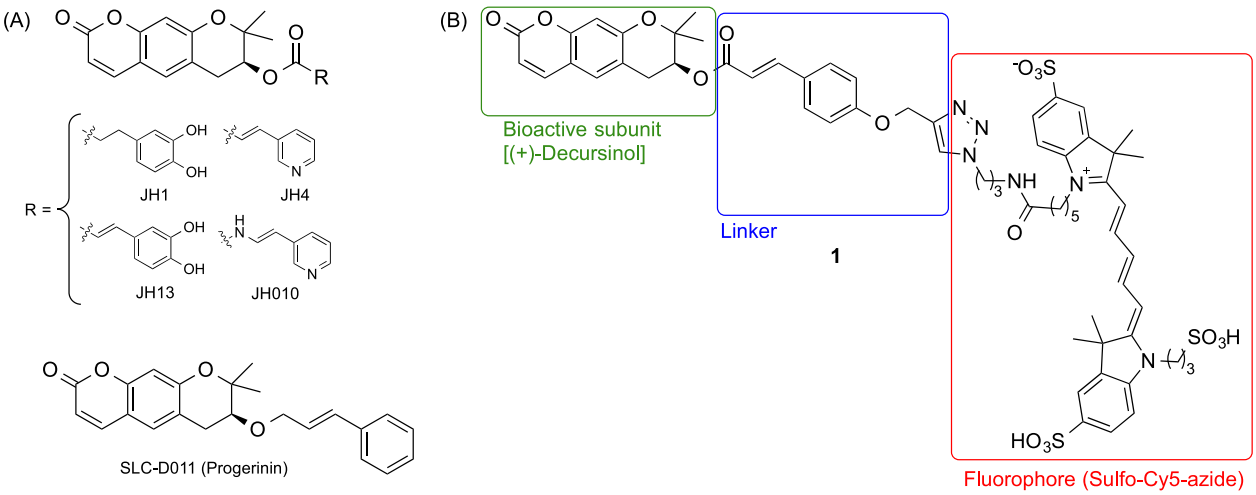

Fig. 1. (A) Representative described progerin ligands. (B) Structure of designed probe **1**.

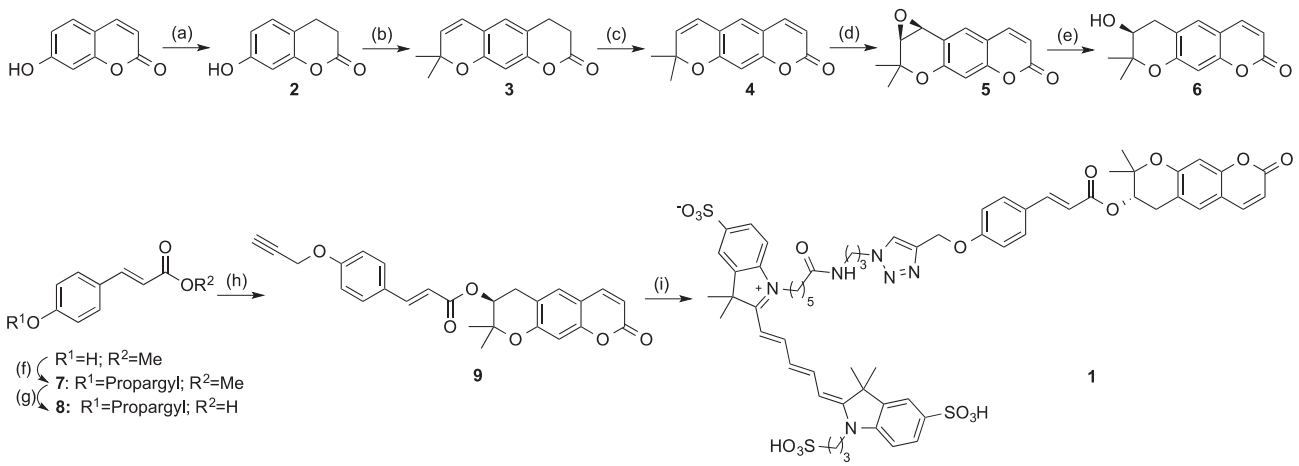

Scheme 1. Synthesis of fluorescent probe 1[a]. [a]Reagents and conditions: (a) H_2, Pd/C 10 %, H-Cube 0.3 mL/min, atmospheric pressure, 40 °C, 99 %; (b) 3-methyl-2-butenal, $PhB(OH)_2$, propionic acid, toluene, MW, 160 °C, 4 h, 64 %; (c) DDQ, toluene, MW, 220 °C, 1.5 h, 92 %; (d) Jacobsen's (*S,S*)-salen-Mn(III) cat., household bleach, Na_2HPO_4, NaOH, dichloromethane, 0 °C to rt, 8 h, 83 %; (e) ZnI_2, $NaBH_4$, dichloroethane, 55 °C, 10 h, 86 %; (f) propargyl bromide, K_2CO_3, KI, acetonitrile, reflux, 1 h, 92 %; (g) i) Aq. NaOH 2 M, ethanol, reflux, 1 h; (ii) Aq. HCl 3 M, 0 °C, 5 min, 99 %; (h) **6**, DCC, DMAP, dichloromethane, rt, 16 h, 69 %; (i) Sulfo-Cy5 azide, $CuSO_4{\cdot}5H_2O$, sodium ascorbate, dimethylformamide (DMF):water (1:1), rt, 16 h, 70 %.

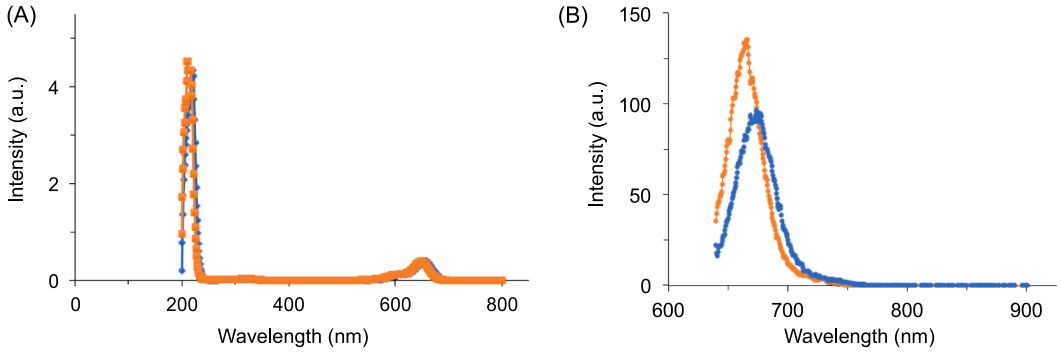

Fig. 2. Spectroscopic characterization of probe **1**. (A) Absorption and (B) emission spectra for compound **1** (5 μM) in ethanol (blue) and PBS (orange). (For interpretation of the references to colour in this figure legend, the reader is referred to the web version of this article.)

emitting in non-overlapping areas.

To ensure cellular target engagement, binding of probe **1** to progerin was assessed by cellular thermal shift assay (CETSA) in progerin-expressing *Lmna*$^{G609G/G609G}$ cell homogenates. This experiment is based on the increase in thermal stability of a protein upon ligand binding, which is revealed by differential protein denaturation upon exposure to heat [31]. Accordingly, progerin-expressing cell homogenates were incubated with compound **1** and the levels of non-denatured progerin determined by western blotting (Fig. 3A). Quantification of the intensity of the bands at the different temperatures in the presence and absence of compound allowed us to generate the corresponding melting curves (Fig. 3B). The rightward shift observed in the melting curve of progerin induced by compound **1** is due to an increase in its melting temperature (T_m), which increased in about 1.5 °C compared to the vehicle-treated cells. This result indicates a direct interaction between compound **1** and progerin.

The affinity of compound **1** for progerin is similar to the one exhibited by progerinin (SLC-D011, Fig. 1), [9,32] synthesized as

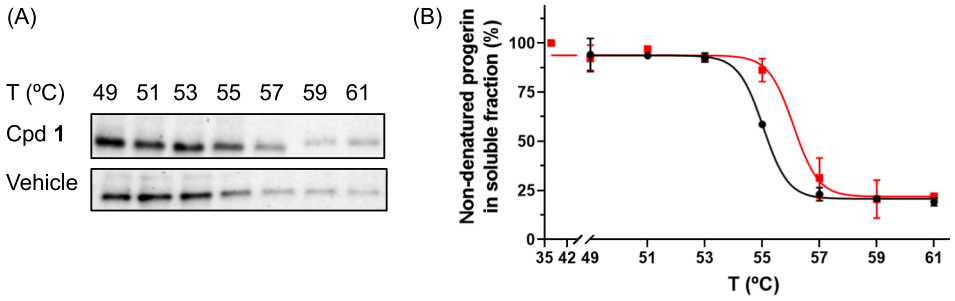

Fig. 3. (A) Representative progerin immunoblotting of the soluble fraction of *Lmna*$^{G609G/G609G}$ cell homogenates treated with 50 μM of compound **1** or vehicle and heat-shocked at the indicated temperature. (B) Thermal denaturation curves of progerin in the presence of vehicle (black) or compound **1** (red) showing thermal stabilization, indicative of direct interaction between progerin and compound **1**. Curves are generated and fitted using a four-parameter non-linear regression curve fit in GraphPad Prism. Symbols and associated error bars (when not enclosed by the symbol) represent average ± SD from at least two independent experiments carried out in duplicate. (For interpretation of the references to colour in this figure legend, the reader is referred to the web version of this article.)

described in the experimental section, as suggest the similar increase in progerin T_m observed in the CETSA analysis (ΔT_m = 1.5 °C, Fig. 4A,B), and higher than the affinity of (+)-decursinol for progerin (ΔT_m = 0.3 °C, Fig. 4C,D).

2.3. Validation of probe 1 in the cellular model of progeria

Once confirmed that the probe was able to bind progerin, we assessed its potential for the visualization of this protein in mouse progeroid cells using confocal experiments. Up to this moment, different genetically modified mouse models have been described. Among them, the *Zmpste24*$^{-/-}$ mouse was one the earliest models to be described [33,34]. These mice are characterized by the development of kyphosis and spontaneous bone fractures in multiple locations, but they only showed partial heart alterations that are characteristic of progeria patients. Later on, a mouse heterozygous for a human transgene with the G608G mutation in LMNA (p.G608G/+) was reported [35]. This model exhibited the progressive vascular abnormalities that are the main causes of lethality in HGPS patients but lacked the rest of the phenotypic features observed in human patients. More recently, and aimed at better recapitulation of all the alterations present in HGPS patients, a *Lmna*$^{G609G/G609G}$ homozygous mouse model was generated [36]. These mice accumulate progerin, present histological and transcriptional alterations characteristic of progeroid models, and phenocopy the main clinical manifestations of human HGPS, including shortened life span and bone and cardiovascular aberrations, and probably represent the most reliable progeria mouse model. Hence, fibroblasts from *Lmna*$^{G609G/G609G}$ mice were cultured and incubated in the presence of compound **1**. The obtained results show that compound **1** is able to label *Lmna*$^{G609G/G609G}$ fibroblasts in a dose-dependent manner (Fig. 5).

Next, we checked the specificity of the labeling by carrying out parallel experiments in the presence of an excess of the progerin ligands (+)-decursinol (**6**) and progerinin. As expected, simultaneous incubation of the probe in the presence of an excess of these compounds abolished labeling (Fig. 6A). We also confirmed that the fluorophore itself (sulfo-Cy5-azide, labeled as Cy5 in Fig. 6) did not show any significant fluorescence up to concentrations of 5 μM, indicating that binding to progerin is driven by the presence of the bioactive subunit. Conversely, neither progerinin nor (+)-decursinol by themselves, under the same conditions as those used for the rest of the images, exhibited significant fluorescence, as shown in the upper panel of Fig. 6A. Finally, we assessed whether probe **1** could discriminate between progeroid cells and normal cells using *Lmna*$^{G609G/G609G}$ and wild type mouse fibroblasts. Pleasantly, the obtained results (Fig. 6B) support that probe **1** is able to differentiate progeroid *Lmna*$^{G609G/G609G}$ cells, with high progerin expression, from *Lmna*$^{+/+}$ mouse fibroblasts, which do not express significant levels of progerin.

3. Conclusions

In this work we design and characterize compound UCM-23079, the first fluorescent probe for the direct visualization of progerin in native cells. This probe is based on (+)-decursinol, a natural product with affinity for progerin, and it represents the first small-molecule tool suitable for the visualization of progerin in cells of the mouse model of the disease, an unmet need of the currently commercially available antibodies. These can be used to visualize progerin by western blot or in immunocytochemical studies in human cells, but not in mouse cells. This

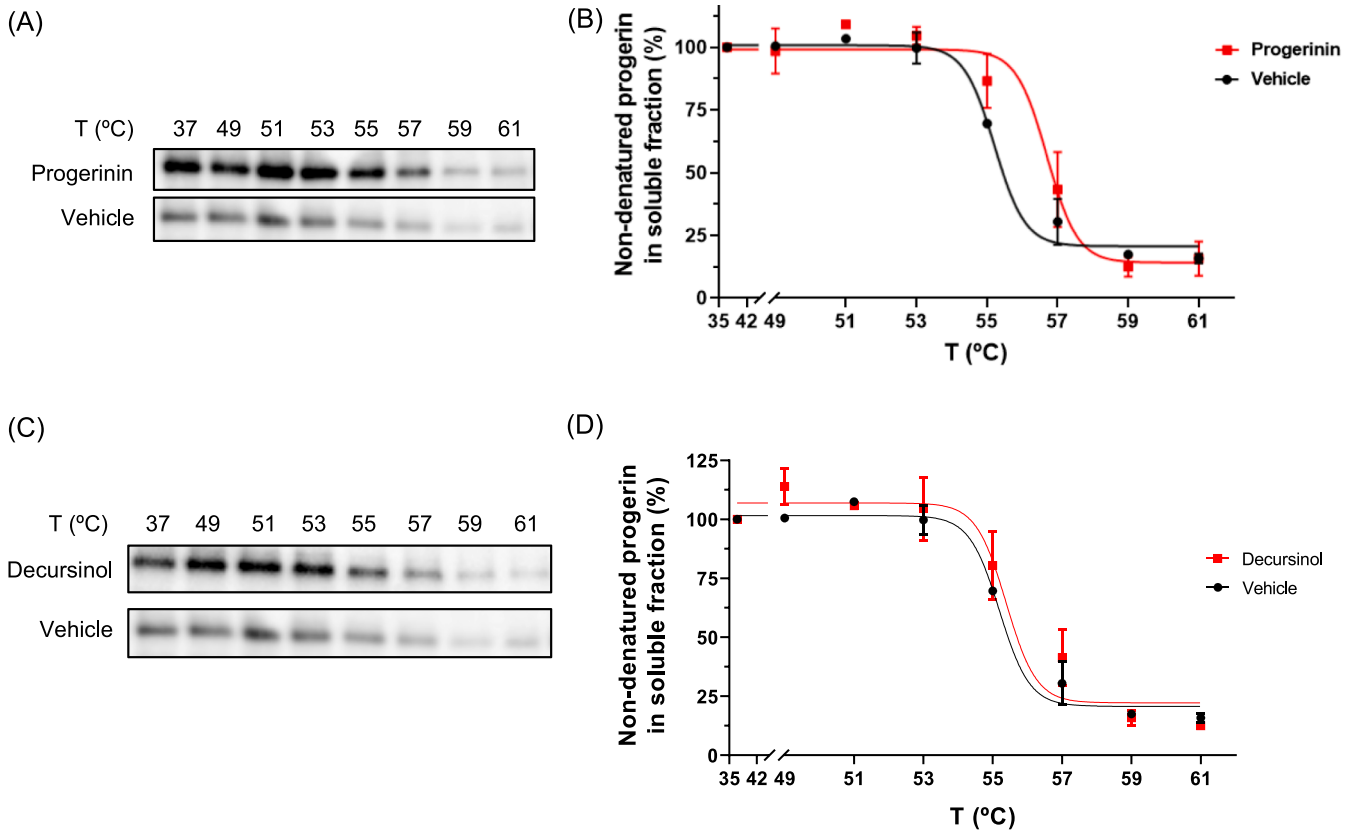

Fig. 4. (A, C) Representative progerin immunoblotting of the soluble fraction of *Lmna*$^{G609G/G609G}$ cell homogenates treated with 50 μM of progerinin or (+)-decursinol as indicated in the figure and heat-shocked at the indicated temperature. (B, D) Thermal denaturation curves of progerin in the presence of vehicle (black) or progerinin or (+)-decursinol (red) as indicated in the figure. Curves are generated and fitted using a four-parameter non-linear regression curve fit in GraphPad Prism. Symbols and associated error bars (when not enclosed by the symbol) represent average ± SD from at least two independent experiments carried out in duplicate. (For interpretation of the references to colour in this figure legend, the reader is referred to the web version of this article.)

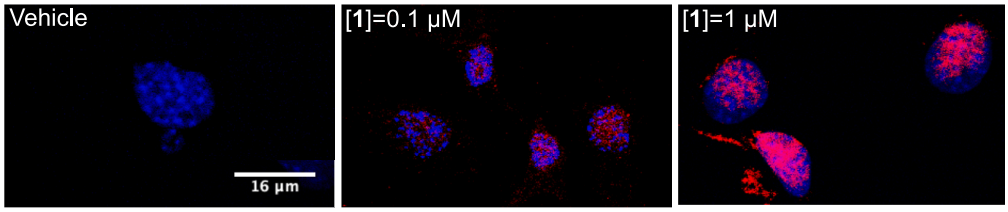

Fig. 5. Probe **1** labels progerin in a dose-dependent manner in *Lmna*$^{G609G/G609G}$ fibroblasts. Cells were incubated with vehicle (left panel) or probe **1** at 0.1 μM (middle panel) or at 1 μM (right panel). Cells were incubated in the presence of vehicle (0.1 % DMSO) or compound for 10 min, washed, fixed, mounted, and then observed by confocal microscopy. All samples were imaged under the same conditions by using an inverted fluorescence microscope (Olympus FV1200 confocal microscope with a UPLSAPO60XO, NA:1.35, objective) and are representative of two or three independent experiments. Nuclei were stained with Hoechst 33342 and are shown in blue. Bar: 16 μm. (For interpretation of the references to colour in this figure legend, the reader is referred to the web version of this article.)

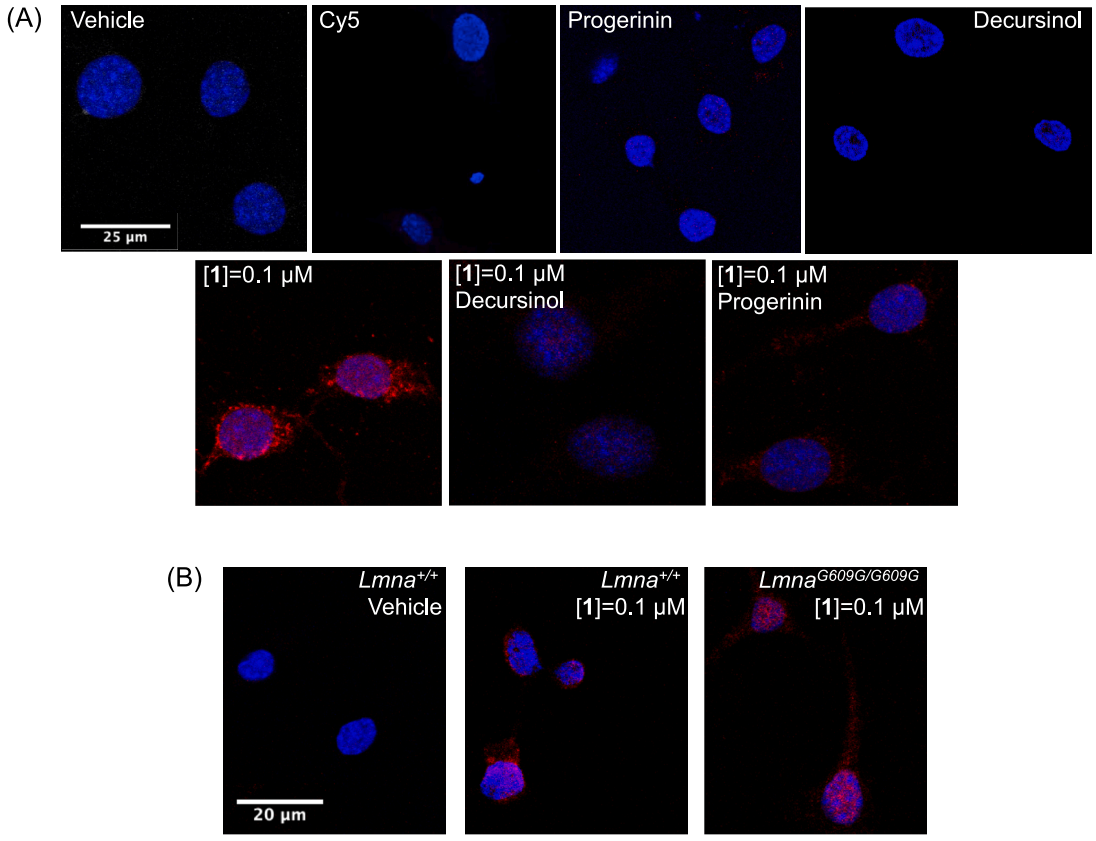

Fig. 6. Specificity of the labeling of probe **1**. (A) *Lmna*$^{G609G/G609G}$ mouse fibroblasts were incubated with vehicle (0.1 % DMSO), fluorophore sulfo-Cy5-azide (Cy5, 5 μM), progerinin (50 μM), (+)-decursinol (250 μM) or with probe **1** alone or in the presence of an excess of the progerin ligands progerinin (50 μM) or (+)-decursinol (250 μM) as indicated in the images. Bar: 25 μm. (B) *Lmna*$^{+/+}$ or *Lmna*$^{G609G/G609G}$ mouse fibroblasts were incubated with vehicle (0.1 % DMSO) or probe **1** (0.1 μM). Bar: 20 μm. After incubation, cells were washed, fixed, mounted, and then observed by confocal microscopy. All samples were imaged under the same conditions by using an inverted fluorescence microscope (Olympus FV1200 confocal microscope with a UPLSAPO60XO, NA: 1.35, objective) and are representative of two or three independent experiments. Nuclei were stained with Hoechst 33342 and are shown in blue. (For interpretation of the references to colour in this figure legend, the reader is referred to the web version of this article.)

limitation is important because it slows down the early preclinical validation of new therapeutic approaches, since a robust effect in the levels of progerin in the different cells and tissues of the mouse model is required (or at least highly desirable) for the advancement to clinical stages. Hence, probe **1** (UCM-23079) adds to the current arsenal of tools for the study of progerin with the aim of contributing to the translation of basic research findings towards the eventual approval of new therapeutic options for progeria patients.

4. Experimental section

4.1. Synthesis

Unless otherwise stated, the starting materials, reagents, and solvents were purchased as high-grade commercial products from Merck Sigma-Aldrich, ABCR, Acros, Biotage, Fluka, Lancaster, Scharlab, or Panreac. Dichloromethane (DCM), diethyl ether and tetrahydrofuran (THF) were dried using a Pure Solv^{TM} Micro 100 Liter solvent purification system. Alcohol-free chloroform was obtained by washing with water, drying over $MgSO_4$, filtration and distillation over P_2O_5. All non-aqueous reactions were performed under an argon or nitrogen atmosphere in oven-dried glassware. Reactions under MW irradiation were

performed in a Biotage Initiatior 2.5 reactor, and hydrogenation reactions were carried out in a ThalesNano H-Cube® HC 2-SS continuous-flow hydrogenation reactor using CatCart® catalyst cartridges. Analytical thin-layer chromatography (TLC) was run on Merck silica gel plates (Kieselgel 60F-254), with detection by UV light (λ = 254 nm), ninhydrin solution, ethanolic solution of 6 % (w/v) vanillin and 1.5 % (v/v) commercial sulfuric acid or 10 % phosphomolybdic acid solution in ethanol. Flash chromatography was performed on glass column using silica gel type 60 (particle size 230–400 mesh, Merck), or on a Biotage Selekt system, using silica gel cartridges (Biotage Sfär Silica D, particle size 60 μm). Compounds were solids except for those whose melting points (m.p.) are not reported, which were oils. M.p. were determined on a Stuart Scientific electrothermal apparatus. Optical rotation [α] was measured on an Anton Paar MCP 100 modular circular polarimeter using a sodium lamp (λ = 589 nm) with a 1 dm path length; concentrations (*c*) are given as g/100 mL. Infrared (IR) spectra were measured on a Bruker Tensor 27 instrument equipped with a Specac ATR accessory of 5200–650 cm^{-1} transmission range; frequencies (*ν*) are expressed in cm^{-1}. ^{1}H- and ^{13}C NMR spectra were recorded on a Bruker Avance III 700 MHz (^{1}H, 700 MHz; ^{13}C, 175 MHz), Bruker Avance 500 MHz (^{1}H, 500 MHz; ^{13}C, 125 MHz) or Bruker DPX 300 MHz (^{1}H, 300 MHz; ^{13}C, 75 MHz) instrument at room temperature (rt) at the Universidad Complutense de Madrid's NMR core facility. Chemical shifts (δ) are expressed in parts per million relative to the residual solvent peak ^{1}H and ^{13}C nucleus (acetone-*d*$_6$: δ_H = 2.05, δ_C = 29.84; $CDCl_3$: δ_H = 7.26, δ_C = 77.16; methanol-*d*$_4$: δ_H = 3.31, δ_C = 49.00); coupling constants (*J*) are in hertz (Hz). The following abbreviations are used to describe peak patterns when appropriate: s (singlet), d (doublet), t (triplet), q (quartet), qt (quintuplet), and m (multiplet). 2D NMR experiments (H,H-COSY, HMQC, HSQC, and HMBC) of representative compounds were carried out to assign protons and carbons of the new structures. High resolution mass spectrometry (HRMS) was carried out on a FTMS Bruker APEX Q IV spectrometer in electrospray ionization (ESI) or matrix-assisted laser desorption/ionization (MALDI) mode at Universidad Complutense de Madrid's mass spectrometry core facility. For all final compounds, purity was determined by HPLC-MS, and satisfactory chromatograms confirmed a purity of at least 95 % for all tested compounds. HPLC-MS analysis was performed using an Agilent 1200LC-MSD VL instrument. LC separation was achieved with an Eclipse XDB-C18 column (5 μm, 4.6 mm x 150 mm), together with a guard column (5 μm, 4.6 mm x 12.5 mm) with a flow rate of 0.5 mL/min. Retention time (R_t) is expressed in minutes. The gradient mobile phase consisted of A (95:5 water/acetonitrile) and B (5:95 water/acetonitrile) with 0.1 % formic acid as solvent modifier. The gradient started at 0 % B (for 5 min), increased linearly to 90 % B over the course of 10 min, and up to 100 % B for 7 min more, before being kept isocratic at 100 % B for 4 min and decreased to 0 % B for the final 4 min (total run time = 30 min). Spectra were acquired in positive or negative ionization mode from 100 to 1200 *m/z* and in UV-mode at four different wavelengths (210, 230, 254, and 280 nm). MS analysis was performed with an ESI source. The capillary voltage was set to 3.0 kV and the fragmentor voltage was set at 25 eV. The drying gas temperature was 350 °C, the drying gas flow was 10 L/min, and the nebulizer pressure was 20 psi.

4.1.1. Synthesis of 7-hydroxy-3,4-dihydro-2H-1-benzopyran-2-one (2)

Umbelliferone (500 mg, 3.09 mmol) was dissolved in absolute ethanol (50 mL) and hydrogenated in an H-Cube® continuous flow hydrogenation reactor with a 10 % palladium-on-carbon catalyst at 0.3 mL/min, 40 °C and atmospheric pressure. The obtained crude was concentrated under vacuum, yielding a brownish solid, which was used without further purification in the next step (505 mg, 3.08 mmol, 99 % yield). **Rf:** 0.64 (hexane/ethyl acetate, 3/2). **m.p.:** 133–134 °C (*lit.* 132–133 °C) [37]. **IR (ATR, cm^{-1}):** 3285 (*ν* O—H), 1721 (*ν* C═O), 1249 (*ν* C-CO-O), 1143 (*ν* O—C—C). **^{1}H NMR (300 MHz, Acetone-*d*$_6$):** *δ* 2.68 – 2.80 (m, 2H), 2.87 – 2.98 (m, 2H), 6.48 (d, *J* = 2.4 Hz, 1H), 6.60 (dd, *J* = 8.2, 2.4 Hz, 1H), 7.07 (d, *J* = 8.2 Hz, 1H), 8.56 (s, 1H). **^{13}C NMR (75 MHz, Acetone-*d*$_6$):** *δ* 23.5, 30.0, 104.3, 112. 114.8, 129.6, 153.8, 158.2, 168.7. **[M + H]$^{+}$:** 165.1. **R$_t$:** 10.31.

4.1.2. Synthesis of 8,8-dimethyl-3,4-dihydro-2H,8H-benzo[1,2-b:5,4-b']dipyran-2-one (3)

A solution of lactone **2** (250 mg, 1.52 mmol), phenylboronic acid (464 mg, 3.81 mmol, 2.5 equiv.) in toluene (5.4 mL) and propionic acid (10.3 mL, 17.1 mmol, 90 equiv.) was slightly heated to favour solubility of the compounds and stirred for 5 min. Then, 3-methyl-2-butenal (0.6 mL, 6.09 mmol, 4 equiv.) was added, and the mixture was stirred at 160 °C for 4 h under MW conditions. The obtained crude was basified with saturated aqueous solution of sodium carbonate and extracted three times with ethyl acetate. The combined organic solutions were washed two times with water and brine, dried over anhydrous sodium sulfate, filtered, and concentrated under vacuum. The solid residue was purified by column chromatography using an elution gradient of hexane to hexane/ethyl acetate 9/1, to obtain pure compound **3** as a yellow pale solid (224 mg, 0.97 mmol, 64 % yield). **Rf:** 0.66 (hexane/ethyl acetate, 3/2). **m.p.:** 149–151 °C. **IR (ATR, cm^{-1}):** 1770 (*ν* C═O), 1621 (*ν* C═C), 1119 (*ν* O—C—C). **^{1}H NMR (300 MHz, $CDCl_3$):** *δ* 1.42 (s, 6H), 2.69 – 2.81 (m, 2H), 2.82 – 2.95 (m, 2H), 5.58 (d, *J* = 9.8 Hz, 1H), 6.26 (dd, *J* = 9.8, 0.7 Hz, 1H), 6.50 (d, *J* = 0.7 Hz, 1H), 6.77 (s, 1H). **^{13}C NMR (75 MHz, $CDCl_3$):** *δ* 23.2, 28.0 (2C), 29.6, 76.7, 105.4, 114.5, 118.0, 121.4, 125.2, 130.5, 152.2, 153.1, 168.7. **[M + H]$^{+}$:** 231.1. **R$_t$:** 13.52.

4.1.3. Synthesis of 8,8-dimethyl-2H,8H-benzo[1,2-b:5,4-b']dipyran-2-one (xanthyletin, 4)

A mixture of compound **3** (180 mg, 0.78 mmol), DDQ (620 mg, 2.74 mmol, 3.5 equiv.) and toluene (11 mL) was stirred at 220 °C for 1.5 h under MW. The reaction crude was quenched with aqueous solution of sodium bicarbonate. Then, the obtained mixture was filtered and the resulting solution extracted three times with ethyl acetate. The combined organic solutions were washed three times with water and brine, dried over anhydrous sodium sulfate, filtered, and concentrated under vacuum. The residue was purified by chromatography with a Biotage® Selekt using an elution gradient of hexane/ethyl acetate 9/1 to ethyl acetate, yielding xanthyletin (**4**) as an orange solid (164 mg, 0.72 mmol, 92 %). **Rf:** 0.49 (hexane/ethyl acetate, 2/1). **m.p.:** 87–89 °C (*lit.* 88–90 °C) [38]. **^{1}H NMR (300 MHz, $CDCl_3$):** *δ* 1.46 (s, 6H), 5.69 (d, *J* = 9.9 Hz, 1H), 6.22 (d, *J* = 9.4 Hz, 1H), 6.34 (d, *J* = 9.8 Hz, 1H), 6.72 (s, 1H), 7.04 (s, 1H), 7.57 (d, *J* = 9.4 Hz, 1H). **^{13}C NMR (75 MHz, $CDCl_3$):** *δ* 28.5 (2C), 77.9, 104.6, 112.9, 113.2, 118.7, 120.9, 124.9, 131.4, 143.5, 155.6, 157.0, 161.3. **[M + H] +:** 229.1. **R$_t$:** 13.37. The spectroscopic data are consistent with those reported in reference [38].

4.1.4. Synthesis of (1aS,9bS)-2,2-dimethyl-1a,9b-dihydro-2H,6H-oxireno[d]benzo[1,2-b:5,4-b]dipyran-6-one (5)

To a solution of Jacobsen's catalyst (*S,S*)-(+)-salen-Mn(III) (2.8 mg, 4.4 μmol, 0.02 equiv.) and xanthyletin (**4**) (50 mg, 0.22 mmol, 1 equiv.) in DCM (1 mL) in an ice bath was added a solution of commercial sodium hypochlorite and sodium dihydrogen phosphate (1.5 mL, 7 mL/mmol). This mixture was prepared with 14.3 mL of commercial household bleach diluted with 5.7 mL of a 0.05 M Na_2HPO_4 solution, and the pH of the resulting solution was adjusted to pH 11.3 by addition of 1 M NaOH solution. The reaction was stirred at 0 °C for ten minutes and then let to reach rt and stirred for additional 6 h. After this time, DCM was added, and the organic phase was extracted. The organic extracts were washed two times with water and brine, dried over anhydrous sodium sulfate, filtered and concentrated under vacuum. The residue was purified by column chromatography using an elution gradient of hexane/ethyl acetate 9/1 to hexane/ethyl acetate 3/2, to give of the desired epoxide as a white solid (35 mg, 0.14 mmol, 65 %). $[\alpha]_D^{25} = -272.0$ (*c* = 1, chloroform) (*lit.* $[\alpha]_D^{24} = -274.7$) [29]. **Rf:** 0.40 (hexane/ethyl acetate, 3/2). **m.p.:** 135–137 °C (*lit.* 135–140 °C) [38]. **IR (ATR, cm^{-1}):** 1730 (*ν* C═O), 1625 (*ν* C═C), 1119 (*ν* O—C—C). **^{1}H NMR (300 MHz, $CDCl_3$):** *δ* 1.30 (s,

3H), 1.60 (s, 3H), 3.53 (d, $J = 4.4$ Hz, 1H), 3.96 (d, $J = 4.4$ Hz, 1H), 6.27 (d, $J = 9.5$ Hz, 1H), 6.76 (s, 1H), 7.45 (s, 1H), 7.63 (d, $J = 9.5$ Hz, 1H). **^{13}C NMR (75 MHz, CDCl3):** δ 23.2, 25.6, 50.3, 62.1, 74.7, 106.3, 113.2, 114.0, 117.4, 129.0, 143.0, 156.2 (2C), 160.9. **[M + H] +:** 245.1. **R_t:** 10.13. The spectroscopic data are consistent with those reported in reference [38].

4.1.5. Synthesis of (7S)-7-hydroxy-8,8-dimethyl-7,8-dihydro-2H,6H-benzo[1,2-b:5,4-b́]dipyran-2-one ((+)-decursinol, 6)

To a flask was added a solution of epoxide **5** (40 mg, 0.16 mmol, 1 equiv.) in DCE (1.5 mL) and zinc iodide (209 mg, 0.66 mmol, 4 equiv.). Then, sodium borohydride (25 mg, 0.66 mmol, 4 equiv.) was added, and the mixture was stirred at 55 °C for 16 h. After this time, the reaction was quenched with an aqueous solution of HCl 1 M and the organic phase was extracted twice with DCM. The organic extracts were washed one time with water and brine, dried over anhydrous sodium sulfate, filtered and concentrated under vacuum. The residue was purified by column chromatography using an elution gradient of hexane/ethyl acetate 8/2 to hexane/ethyl acetate 3/2, to obtain pure (+)-decursinol (**6**) as a white solid (35 mg, 0.14 mmol, 86 % yield). $[\alpha]_D^{25} = +12.3$ ($c = 1$, chloroform) (*lit.* $[\alpha]_D^{26} = +10.3$, $c = 1$, chloroform, [28]). **Rf:** 0.56 (ethyl acetate). **m.p.:** 165–167 °C (*lit.*167–170 °C) [28]. **^{1}H NMR (300 MHz, $CDCl_3$):** δ 1.36 (s, 3H), 1.39 (s, 3H), 2.83 (ddd, $J = 16.7$, 5.9, 1.1 Hz, 1H), 3.11 (ddd, $J = 16.7$, 4.8, 1.2 Hz, 1H), 3.87 (t, $J = 5.3$ Hz, 1H), 6.22 (d, $J = 9.4$ Hz, 1H), 6.78 (s, 1H), 7.18 (t, $J = 1.2$ Hz, 1H), 7.57 (d, $J = 9.4$ Hz, 1H). **^{13}C NMR (75 MHz, $CDCl_3$):** δ 22.2, 25.2, 30.8, 69.3, 78.3, 104.9, 113.1, 113.5, 116.6, 129.1, 143.3, 154.3, 156.6, 161.5. **R_t:** 11.00. The spectroscopic data are consistent with those reported in reference [28].

4.1.6. Synthesis of methyl (2E)-3-{4-[(prop-2-yn-1-yl)oxy]phenyl}prop-2-enoate (7)

A mixture of methyl (*E*)-3-(4-hydroxyphenyl)acrylate (500 mg, 2.80 mmol, 1 equiv.), potassium carbonate (775 mg, 5.60 mmol, 2 equiv.) and potassium iodide (93 mg, 0.56 mmol, 0.2 equiv.) in acetonitrile (22 mL, 7.9 mL/mmol) was stirred for 1 h. Then, propargyl bromide (0.42 mL, 4.5 mmol, 1.6 equiv.) was added, and the reaction was refluxed for 3 h. The solvent was evaporated under vacuum, water was added, and the mixture was extracted three times with ethyl acetate. The organic layers were combined and washed two times with brine, dried over anhydrous sodium sulfate, filtered and concentrated under vacuum, yielding methyl ester **7** as a white solid (556 mg, 2.57 mmol, 92 % yield), which was used without further purification in the next step. **Rf:** 0.65 (hexane/ethyl acetate, 3/2). **m.p.:** 76–77 °C. **IR (ATR, cm^{-1}):** 3254 (ν H-C≡C), 2129 (ν C≡C), 1694 (ν C═O), 1600 (ν C═C), 1244 (ν C—O—C), 1170 (ν O—C—C). **^{1}H NMR (300 MHz, $CDCl_3$):** δ 2.54 (t, $J =$ 2.4 Hz, 1H), 3.79 (s, 3H), 4.72 (d, $J = 2.4$ Hz, 2H), 6.32 (d, $J = 16.0$ Hz, 1H), 6.93 – 7.04 (m, 2H), 7.43 – 7.54 (m, 2H), 7.65 (d, $J = 16.0$ Hz, 1H). **^{13}C NMR (75 MHz, $CDCl_3$):** δ 51.8, 56.0, 76.1, 78.2, 115.4 (2C), 116.0, 128.1, 129.8 (2C), 144.4, 159.4, 167.8. **[M + H] $^+$:** 217.1. **R_t:** 12.89. The ^{1}H-RMN data are consistent with those reported in reference [39].

4.1.7. Synthesis of (2E)-3-{4-[(prop-2-yn-1-yl)oxy]phenyl}prop-2-enoic acid (8)

To a solution of the corresponding methyl ester **7** (100 mg, 0.46 mmol, 1 equiv.) in ethanol (4.5 mL/mmol), an aqueous solution of NaOH (2 M, 6 equiv.) was added, and the mixture was refluxed for 1 h. After this time, an aqueous solution of HCl 3 M was added until pH 1–2. The formed solid was collected by filtration and washed with cold water, yielding the corresponding carboxylic acid as a white solid (92 mg, 99 %). **Rf:** 0.27 (hexane/ethyl acetate, 3/2). **m.p.:** 178–179 °C. **IR (ATR, cm^{-1}):** 3274 (ν H-C≡C), 2815 (ν sb COO-H), 2129 (ν C≡C), 1678 (ν C═O), 1622 (ν C═C), 1217 (ν C—O—C). **^{1}H NMR (300 MHz, Acetone-d_6):** δ 3.12 (t, $J = 2.4$ Hz, 1H), 4.86 (d, $J = 2.5$ Hz, 2H), 6.42 (d, $J =$ 16.0 Hz, 1H), 7.07 (d, $J = 8.9$ Hz, 2H), 7.64 (d, $J = 16.0$ Hz, 1H), 7.66 (d, $J = 8.5$ Hz, 2H), 10.60 (s, 1H). **^{13}C NMR (75 MHz, Acetone-d_6):** δ 56.4, 77.3, 79.4, 116.1 (2C), 117.1, 128.8, 130.6 (2C), 145.0, 160.3, 167.9. **[M + H] $^+$:** 203.1. **R_t:** 11.34.

4.1.8. Synthesis of (7S)-8,8-dimethyl-2-oxo-7,8-dihydro-2H,6H-benzo[1,2-b:5,4-b́]dipyran-7-yl (2E)-3-{4-[(prop-2-yn-1-yl)oxy]phenyl}prop-2-enoate (9)

Carboxylic acid **8** (12.3 mg, 61 μmol, 1.5 equiv.), DCC (16.8 mg, 81 μmol, 2 equiv.) and DMAP (2 mg, 16 μmol, 0.4 equiv.) in DCM (0.7 mL) were added to a flask. Then, a solution of (+)-decursinol (**6**) (10 mg, 41 μmol, 1 equiv.) in DCM (0.7 mL) was added, and the mixture was stirred at rt for 16 h. After this time, the solution was filtered, cooled at −20 °C, and filtered twice to remove the byproduct 1,3-dicyclohexylurea. The solution was concentrated under vacuum and the residue was purified by column chromatography using an elution gradient of hexane/ethyl acetate 8/2 to hexane/ethyl acetate 1/1, yielding the compound **9** as white solid (12 mg, 27.9 μmol, 69 % yield).$[\alpha]_D^{25} = +7.0$ ($c = 1$, chloroform). **Rf:** 0.78 (ethyl acetate). **m.p.:** 129–130 °C. **IR (ATR, cm^{-1}):** 3288 (ν H-C≡C), 1710, 1705 (ν C═O), 1624, 1600 (C═C), 1128 (ν C—O—C). **^{1}H NMR (300 MHz, $CDCl_3$):** δ 1.39 (s, 3H), 1.43 (s, 3H), 2.53 (t, $J = 2.4$ Hz, 1H), 2.93 (dd, $J = 17.3$, 4.7 Hz, 1H), 3.23 (dd, $J = 17.1$, 4.8 Hz, 1H), 4.71 (d, $J = 2.4$ Hz, 2H), 5.18 (t, $J = 4.8$ Hz, 1H), 6.23 (d, $J =$ 9.4 Hz, 1H), 6.29 (d, $J = 15.9$ Hz, 1H), 6.82 (s, 1H), 6.96 (d, $J = 8.8$ Hz, 2H), 7.17 (s, 1H), 7.46 (d, $J = 8.8$ Hz, 2H), 7.58 (d, $J = 9.5$ Hz, 1H), 7.63 (d, $J = 15.9$ Hz, 1H). **^{13}C NMR (75 MHz, $CDCl_3$):** δ 23.5, 25.1, 28.0, 55.9, 70.2, 76.1, 76.9, 78.1, 105.0, 113.1, 113.5, 115.4 (2C), 115.5, 115.9, 127.8, 128.9, 130.0 (2C), 143.3, 145.4, 154.4, 156.6, 159.6, 161.4, 167.0. **[M + H] $^+$:** 431.1. **R_t:** 13.96.

4.1.9. Synthesis of 2-((1E,3E)-5-((E)-3,3-dimethyl-5-sulfo-1-(3-sulfopropyl)indolin-2-ylidene)penta-1,3-dien-1-yl)-3,3-dimethyl-1-(6-oxo-6-((3-(4-((4-((E)-3-oxo-3-(((S)-6,6,8,8-tetramethyl-2-oxo-7,8-dihydro-2H,6H-pyrano[3,2-g]chromen-7-yl)oxy)prop-1-en-yl) phenoxy)methyl)-1H-1,2,3-triazol-1-yl)propyl)amino)hexyl)–3H-indol-1-ium-5-sulfonate (1)

To a mixture of sulfo-Cy5-azide (9.7 mg, 11.6 μmol, 1 equiv.), copper (II) sulfate (1.4, 5.8 μmol, 0.5 equiv.) and sodium ascorbate (2.3 mg, 11.6 μmol, 1 equiv.) in DMF (47 μL, 4 mL/mmol **9**) and water (128 μL, 11 mL/mmol **9**) was added a solution of the compound **9** (5 mg, 11.6 μmol, 1 equiv.) in DMF (82 μL, 7 mL/mmol **9**) and it was stirred at rt for 16 h. The resulting solution was concentrated under vacuum, dissolved in the minimum amount of acetonitrile/water 7/3 and purified by preparative chromatography employing the same mixture as eluent. The obtained residue was dissolved in the same eluent, filtered through HPLC filters (Agilent PTFE 0.2 μm), and the solvent was lyophilized for 16 h to remove water, yielding target compound **1** as a blue solid (8.5 mg, 6.61 μmol, 57 % yield). **Rf:** 0.50 (acetonitrile/water, 7/3). **^{1}H NMR (700 MHz, CD_3OD):** δ 1.39 (s, 3H), 1.41 (s, 3H), 1.42–1.45 (m, 2H), 1.67 (qt, $J = 7.7$ Hz, 2H), 1.72 (s, 12H), 1.83 (qt, $J = 7.5$ Hz, 2H), 2.03 (qt, $J = 6.9$ Hz, 2H), 2.14–2.18 (m, 2H), 2.22 (qt, $J = 7.0$ Hz, 2H), 2.95 (dd, $J = 17.5$, 4.8 Hz, 1H), 2.98 (t, $J = 6.6$ Hz, 2H), 3.14 (t, $J = 6.8$ Hz, 2H), 3.28 (dd, $J = 17.3$, 4.4 Hz, 1H), 4.14 (t, $J = 7.3$ Hz, 2H), 4.32 (t, $J =$ 8.1 Hz, 2H), 4.43 (t, $J = 7.0$ Hz, 2H), 5.20 (m, 3H), 6.23 (d, $J = 9.4$ Hz, 1H), 6.33 (d, $J = 13.7$ Hz, 1H), 6.36 (d, $J = 15.9$ Hz, 1H), 6.47 (d, $J =$ 13.7 Hz, 1H), 6.64 (t, $J = 12.4$ Hz, 1H), 6.76 (s, 1H), 7.02 (d, $J = 8.9$ Hz, 2H), 7.33 (d, $J = 8.1$ Hz, 1H), 7.40 (s, 1H), 7.38–7.42 (m, 1H), 7.53 (d, J = 8.6 Hz, 2H), 7.60 (d, $J = 15.8$ Hz, 1H), 7.85 (d, $J = 9.4$ Hz, 1H), 7.87–7.90 (m, 4H), 8.16 (s, 1H), 8.30 (td, $J = 13.1$, 5.7 Hz, 2H). **^{13}C NMR (175 MHz, CD_3OD):** δ 23.6, 24.0, 25.2, 26.4, 27.2, 27.8 (4C), 28.3, 28.7, 31.1, 36.6, 37.4, 44.1, 45.0, 49.1, 49.2, 50.5, 50.6, 62.4, 71.5, 78.1, 105.0, 105.5, 105.6, 111.6, 111.8, 113.6, 114.4, 116.0, 116.4 (2C), 117.8, 121.4 (2C), 125.8, 128.0, 128.1, 128.2, 128.6, 130.6, 131.2 (2C), 142.5, 142.7, 143.3, 143.4, 144.6, 144.8, 144.9, 145.7, 146.7, 155.4, 156.3 (2C), 158.0, 161.8, 163.4, 168.0, 175.2, 175.5, 175.9. **HRMS: [M + H] $^+$ calculated:** 1263.4248, **[M + H] $^+$ found:** 1263.4242.

4.1.10. Synthesis of (7S)-(+)-8,8-dimethyl-7-(3-phenyl-allyloxy)-7,8-dihydro-6H-pyrano[3,2-g]chromen-2-one (progerinin, SLC-D011)

To a round bottom flask containing cinnamyl alcohol (0.48 mL, 3.73 mmol, 1 equiv.) dissolved in dichloromethane (18.6 mL), triethylamine (0.52 mL, 3.72 mmol, 1 equiv.), DMAP (45.5 mg, 0.37 mmol, 0.1 equiv.), and di-*tert*-butyl-dicarbonate (1.22 g, 5.59 mmol, 1.5 equiv.) were sequentially added. The mixture was stirred for 2 h at rt and was later concentrated under vacuum. The crude product was purified by silica gel column chromatography (ethyl acetate/hexane, 1/30) to obtain *tert*-butyl cinnamyl carbonate as a colorless oil (551 mg, 63 %). *Tert*-butyl cinnamyl carbonate (60 mg, 0.26 mmol, 1.5 equiv.) and **6** (42 mg, 0.17 mmol, 1 equiv.) were added into a 10 mL round bottom flask and the mixture was dried under vacuum for 1 h. The dried mixture was dissolved in anhydrous THF (1.7 mL) under N_2 gas and after bubbling the solution for 1 h, tetrakis(triphenylphosphine)palladium (7.9 mg, 0.007 mmol, 0.04 equiv.) was added to the reaction mixture and was refluxed overnight. The crude was concentrated under reduced pressure and purified by column chromatography (ethyl acetate/hexane, from 1/8 to 1/4) to obtain target compound (19 mg, 0.05 mmol, 31 %) as a white solid.

R_f: 0.51 (hexane/ethyl acetate, 1/1). **m.p.**: 145 °C (*lit.* 143 °C) [32]. **IR (ATR)**: 1728 (ν C═O), 1624 (ν C═O), 1132 (ν C—O), 1076 (ν C—O). **^{1}H NMR (300 MHz, $CDCl_3$)**: δ 1.36 (s, 3H), 1.42 (s, 3H), 2.86 (dd, J = 16.7, 7.1 Hz, 1H), 3.08 (dd, J = 16.6, 5.0 Hz, 1H), 3.59 (dd, J = 7.3, 5.0 Hz, 1H), 4.21 (ddd, J = 12.8, 6.3, 1.4 Hz, 1H), 4.34 (ddd, J = 12.8, 5.9, 1.5 Hz, 1H), 6.20 (d, J = 9.5 Hz, 1H), 6.24–6.34 (m, 1H), 6.59 (d, J = 16.2 Hz, 1H), 6.77 (s, 1H), 7.16 (s, 1H), 7.21–7.44 (m, 5H), 7.56 (d, J = 9.5 Hz, 1H). **^{13}C NMR (75 MHz, $CDCl_3$)**: δ 21.7, 26.0, 27.7, 70.7, 75.8, 78.1, 104.8, 112.8, 113.2, 117.2, 126.0, 126.6 (2C), 128.0, 128.8 (2C), 128.9, 132.8, 136.6, 143.3, 154.3, 156.8, 161.5. **[M + H]$^+$**: 363.2. **R_t**: 16.05. The spectroscopic data are consistent with those reported in reference [32].

4.2. Fluorescence spectroscopy

Absorption spectra were determined using 5 μM solutions of the compound in phosphate buffered saline (PBS) buffer or ethanol at 25 °C on a Shimadzu UV-2550 UV − vis spectrophotometer in 1 cm path length quartz cells. Spectra were recorded between 250 and 700 nm (0.5 nm increments and 0.1 s integration time), and they were corrected for background absorbance by subtracting a blank scan of the buffer solution. Emission spectra were determined for the same solutions on a PerkinElmer LS50B luminescence spectrometer in 1 cm path length quartz cells. The spectra were recorded between 340 and 690 nm (1 nm increments and 0.1 s integration time) with excitation set at the appropriate excitation wavelength. Slit widths were set to 2.5 nm for excitation and emission. All the spectra were corrected for background fluorescence by subtracting a blank scan of the buffer solution.

4.3. CETSA experiments

Progeroid mouse fibroblasts (*Lmna*$^{G609G/G609G}$) were grown as detailed in section 4.4. Cells (2×10^6) were seeded 1 day before the experiment. On the day of the experiment, cells were washed with PBS, detached by treatment with trypsin, and collected by centrifugation at 250*g* and 25 °C for 5 min, washed with PBS (1 × 5 mL) and resuspended in PBS in 0.2 mL microtubes. The cell suspension was homogenized by sonication with 10 pulses (Amplitude 50 %) of 3 s in an ice bath using a Sonoplus mini-20 Ultrasonic Homogenizer. Homogenates were incubated with compound **1** (50 μM) for 60 min at 37 °C or with vehicle. Then, homogenates were transferred to PCR tubes and heat-shocked for 3 min at the appropriate temperature (37 to 61 °C) followed by rapid cooling to 25 °C using a SensoQuest LabCycler Thermocycler (Progen Scientific Ltd). Igepal-630 was then added to the samples (final concentration of 1 % v/v), and the samples were thoroughly mixed and denatured by three cycles of freezing/thawing (immersion in liquid nitrogen for 3 min followed by fast thawing). The non-soluble fraction was separated by centrifugation at 12000*g* for 20 min at 4 °C and the supernatants were transferred to clean microtubes. Then, Laemmli buffer (Bio-Rad) was added and samples were heated at 100 °C for 10 min. Equal protein amounts were separated by SDS-PAGE and transferred to a nitrocellulose membrane (Amersham Protran 0.45 μm) using a wet tank (100 v for 60 min). The membranes were then blocked for 1 h at rt with Tris-buffered saline with 0.05 % v/v Tween20® (TBST) and 5 % BSA, followed by overnight incubation with the primary antibody (1:1000, I1020 SantaCruz sc-376248) at 4 °C. Then, the primary antibody was removed, the membrane was washed three times with TBST and incubated with the secondary antibody (goat anti-mouse HRP conjugate, 1:10000, Bio-Rad) for 1 h at rt. After washing the membrane (six times with TBST), it was incubated with ECL™ Western Blotting Detection Reagents (Cytiva, Amersham) for 3 min and the luminescence signal was detected using a Universal Hood II ChemiDoc XRS + System (Bio-Rad). Signal intensities were determined by quantification of chemiluminescence counts per square millimeter using the Image-Lab software (Bio-Rad). Signals were normalized with respect to the intensity of the soluble fraction obtained at 37 °C, which was established as 100 % non-denatured protein. Curves were generated and fitted using a four-parameter non-linear regression curve fit in GraphPad Prism.

4.4. Cell visualization experiments

Progeroid mouse fibroblasts (*Lmna*$^{G609G/G609G}$) and their wild-type counterparts were kindly donated by Prof. Carlos López Otín (Oviedo University, Spain). Cells were grown in Dulbecco's Modified Eagle medium (DMEM, Invitrogen) supplemented with 10 % heat-inactivated fetal bovine serum (FBS, HyClone), 1 % L-glutamine (Invitrogen), 1 % sodium pyruvate (Invitrogen), 50 U/mL penicillin and 50 μg/mL streptomycin (Invitrogen) in a humidified atmosphere with 5 % CO_2 at 37 °C. For labeling studies, cells were treated with 0.125 % trypsin (Invitrogen) and plated onto glass coverslips in 24-well tissue culture dishes at a density of 20,000 cells/well and cultured under the same conditions as above for an additional 24 to 48 h. Stock solutions of the compounds were prepared in DMSO and then diluted to the final concentration with permeabilization/wash buffer I (R&D Systems, FC005) so that DMSO content was <0.5 %.

For cell labeling, culture media was aspirated and cells were washed with PBS and fixed with 2 % paraformaldehyde for 15 min. Paraformaldehyde was removed and after washing the cells with PBS, they were incubated with compound or vehicle for 10 min at ~20 °C. Afterwards, the buffer solution was removed, cells were washed with PBS and incubated with Hoechst (5 μg/mL in permeabilization buffer) for 15 min at rt for nuclear staining. After washing the cells with PBS, they were mounted on glass slides with Immu-mount (Thermo Scientific). Preparations were observed with an inverted fluorescence microscope (Olympus FV1200) with a UPLSAPO60XO (NA:1.35) objective (Hoechst: excitation: 405 nm and emission: 440–480; Cy5: excitation: 633 nm and emission > 650 nm) at the Universidad Complutense de Madrid's microscopy core facility. For displacement studies, culture media was aspirated and cells were washed with permeabilization/wash buffer I (R&D Systems, FC005) and incubated in the presence of (+)-decursinol or progerinin for 30 min at ~20 °C. Then, probe **1** was added and incubation continued for 10 min. Afterwards, cells were treated as described above for standard visualization experiments.

Author Contributions

The manuscript was written through contributions of all authors. S. O.G. conceived, designed, and supervised research. J.M. and D.F. carried out the synthesis and performed the spectroscopic characterization, target engagement and visualization experiments. All authors have given approval to the final version of the manuscript.

Declaration of Competing Interest

The authors declare that they have no known competing financial interests or personal relationships that could have appeared to influence the work reported in this paper.

Acknowledgements

This work has been supported by the Spanish Ministerio de Ciencia, Innovación y Universidades (grant numbers PID2019-106279RB-I00 and PID2022-138797OB-I00 to S.O.-G. and predoctoral FPU fellowship to J.M., grant number FPU18/05620), The Progeria Research Foundation (grant number PRF 2022-84 to S.O.-G.), and Comunidad de Madrid (Predoctoral fellowship PIPF-2022/SAL-GL-24817 to D.F.). Authors thank Prof. Carlos Lopez-Otin (Oviedo University, Spain) for kindly donating *Lmna*$^{G609G/G609G}$ mouse fibroblasts. Biorender was used to prepare the graphical abstract.

Appendix A. Supplementary data

^{1}H-, ^{13}C-, and 2D (H,H-COSY, HMBC and HMQC or HSQC) NMR spectra of final compounds (**1**, **6**, and progerinin).

Supplementary data to this article can be found online at https://doi.org/10.1016/j.bioorg.2023.106967.

References

[1] A. De Sandre-Giovannoli, R. Bernard, P. Cau, C. Navarro, J. Amiel, I. Boccaccio, S. Lyonnet, C.L. Stewart, A. Munnich, M. Le Merrer, N. Levy, Lamin A truncation in Hutchinson-Gilford progeria, Science 300 (2003) 2055.

[2] M. Eriksson, W.T. Brown, L.B. Gordon, M.W. Glynn, J. Singer, L. Scott, M.R. Erdos, C.M. Robbins, T.Y. Moses, P. Berglund, A. Dutra, E. Pak, S. Durkin, A.B. Csoka, M. Boehnke, T.W. Glover, F.S. Collins, Recurrent de novo point mutations in lamin A cause Hutchinson-Gilford progeria syndrome, Nature 423 (2003) 293–298.

[3] L.B. Gordon, F.G. Rothman, C. Lopez-Otin, T. Misteli, Progeria: a paradigm for translational medicine, Cell 156 (2014) 400–407.

[4] B. Benhamú, M. Martín-Fontecha, H. Vázquez-Villa, M.L. López-Rodríguez, S. Ortega-Gutiérrez, New trends in aging drug discovery, Biomedicines 2022 (2006) 10.

[5] J.P. de Magalhães, Longevity pharmacology comes of age, Drug Discov. Today 26 (2021) 1559–1562.

[6] J. Macicior, B. Marcos-Ramiro, S. Ortega-Gutiérrez, Small-molecule therapeutic perspectives for the treatment of progeria, Int. J. Mol. Sci. 22 (2021) 7190–7200.

[7] I. Benedicto, X. Chen, M.O. Bergo, V. Andrés, Progeria: a perspective on potential drug targets and treatment strategies, Expert Opin. Ther. Targets 26 (2022) 393–399.

[8] B. Marcos-Ramiro, A. Gil-Ordóñez, N.I. Marín-Ramos, F.J. Ortega-Nogales, M. Balabasquer, P. Gonzalo, N. Khiar-Fernández, L. Rolas, A. Barkaway, S. Nourshargh, V. Andrés, M. Martín-Fontecha, M.L. López-Rodríguez, S. Ortega-Gutiérrez, Isoprenylcysteine carboxylmethyltransferase-based therapy for Hutchinson-Gilford Progeria Syndrome, ACS Cent. Sci. 7 (2021) 1300–1310.

[9] S.M. Kang, M.H. Yoon, J. Ahn, J.E. Kim, S.Y. Kim, S.Y. Kang, J. Joo, S. Park, J. H. Cho, T.G. Woo, A.Y. Oh, K.J. Chung, S.Y. An, T.S. Hwang, S.Y. Lee, J.S. Kim, N. C. Ha, G.Y. Song, B.J. Park, Progerinin, an optimized progerin-lamin A binding inhibitor, ameliorates premature senescence phenotypes of Hutchinson-Gilford progeria syndrome, Commun. Biol. 4 (2021) 5.

[10] S.J. Lee, Y.S. Jung, M.H. Yoon, S.M. Kang, A.Y. Oh, J.H. Lee, S.Y. Jun, T.G. Woo, H. Y. Chun, S.K. Kim, K.J. Chung, H.Y. Lee, K. Lee, G. Jin, M.K. Na, N.C. Ha, C. Barcena, J.M. Freije, C. Lopez-Otin, G.Y. Song, B.J. Park, Interruption of progerin-lamin A/C binding ameliorates Hutchinson-Gilford progeria syndrome phenotype, J. Clin. Invest. 126 (2016) 3879–3893.

[11] O. Santiago-Fernandez, F.G. Osorio, V. Quesada, F. Rodriguez, S. Basso, D. Maeso, L. Rolas, A. Barkaway, S. Nourshargh, A.R. Folgueras, J.M.P. Freije, C. Lopez-Otin, Development of a CRISPR/Cas9-based therapy for Hutchinson-Gilford progeria syndrome, Nat. Med. 25 (2019) 423–426.

[12] E. Beyret, H.K. Liao, M. Yamamoto, R. Hernandez-Benitez, Y. Fu, G. Erikson, P. Reddy, J.C. Izpisua Belmonte, Single-dose CRISPR-Cas9 therapy extends lifespan of mice with Hutchinson-Gilford progeria syndrome, Nat. Med. 25 (2019) 419–422.

[13] M.R. Erdos, W.A. Cabral, U.L. Tavarez, K. Cao, J. Gvozdenovic-Jeremic, N. Narisu, P.M. Zerfas, S. Crumley, Y. Boku, G. Hanson, D.V. Mourich, R. Kole, M.A. Eckhaus, L.B. Gordon, F.S. Collins, A targeted antisense therapeutic approach for Hutchinson-Gilford progeria syndrome, Nat. Med. 27 (2021) 536–545.

[14] L.W. Koblan, M.R. Erdos, C. Wilson, W.A. Cabral, J.M. Levy, Z.M. Xiong, U. L. Tavarez, L.M. Davison, Y.G. Gete, X. Mao, G.A. Newby, S.P. Doherty, N. Narisu, Q. Sheng, C. Krilow, C.Y. Lin, L.B. Gordon, K. Cao, F.S. Collins, J.D. Brown, D. R. Liu, In vivo base editing rescues Hutchinson-Gilford progeria syndrome in mice, Nature 589 (2021) 608–614.

[15] M. Puttaraju, M. Jackson, S. Klein, A. Shilo, C.F. Bennett, L. Gordon, F. Rigo, T. Misteli, Systematic screening identifies therapeutic antisense oligonucleotides for Hutchinson-Gilford progeria syndrome, Nat. Med. 27 (2021) 526–535.

[16] M. Suzuki, L.J.B. Jeng, S. Chefo, Y. Wang, D. Price, X. Li, J. Wang, R.J. Li, L. Ma, Y. Yang, X. Zhang, N. Zheng, K. Zhang, D.B. Joseph, H. Shroff, J. Doan, M. Pacanowski, P. Smpokou, K. Donohue, H.V. Joffe, FDA approval summary for lonafarnib (Zokinvy) for the treatment of Hutchinson-Gilford progeria syndrome and processing-deficient progeroid laminopathies, Genet. Med. 25 (2023), 100335.

[17] F.M. Hisama, J. Oshima, Precision medicine and progress in the treatment of Hutchinson-Gilford progeria syndrome, Jama 319 (2018) 1663–1664.

[18] J.I. Scott, Q. Deng, M. Vendrell, Near-infrared fluorescent probes for the detection of cancer-associated proteases, ACS Chem. Biol. 16 (2021) 1304–1317.

[19] M. Soave, S.J. Briddon, S.J. Hill, L.A. Stoddart, Fluorescent ligands: Bringing light to emerging GPCR paradigms, Br. J. Pharmacol. 177 (2020) 978–991.

[20] J. Khiar-Fernández, J. Macicior, B. Marcos-Ramiro, S. Ortega-Gutiérrez, Chemistry for the identification of therapeutic targets: Recent advances and future directions, Eur. J. Org. Chem. 2021 (2021) 1307–1320.

[21] L. Martin-Couce, M. Martin-Fontecha, S. Capolicchio, M.L. Lopez-Rodriguez, S. Ortega-Gutierrez, Development of endocannabinoid-based chemical probes for the study of cannabinoid receptors, J. Med. Chem. 54 (2011) 5265–5269.

[22] L. Martin-Couce, M. Martin-Fontecha, O. Palomares, L. Mestre, A. Cordomi, M. Hernangomez, S. Palma, L. Pardo, C. Guaza, M.L. Lopez-Rodriguez, S. Ortega-Gutierrez, Chemical probes for the recognition of cannabinoid receptors in native systems, Angew. Chem. Int. Ed. Engl. 51 (2012) 6896–6899.

[23] M. Martín-Fontecha, A. Angelina, B. Rückert, A. Rueda-Zubiaurre, L. Martín-Cruz, W. van de Veen, M. Akdis, S. Ortega-Gutiérrez, M.L. López-Rodríguez, C.A. Akdis, O. Palomares, A fluorescent probe to unravel functional features of cannabinoid receptor CB(1) in human blood and tonsil immune system cells, Bioconjug. Chem. 29 (2018) 382–389.

[24] G. Hernández-Torres, E. Enríquez-Palacios, M. Mecha, A. Feliú, A. Rueda-Zubiaurre, A. Angelina, L. Martín-Cruz, M. Martín-Fontecha, O. Palomares, C. Guaza, E. Peña-Cabrera, M.L. López-Rodríguez, S. Ortega-Gutiérrez, Development of a fluorescent bodipy probe for visualization of the Serotonin 5-HT (1A) receptor in native cells of the immune system, Bioconjug. Chem. 29 (2018) 2021–2027.

[25] H. Vázquez-Villa, J.A. González-Vera, B. Benhamú, A. Viso, R. Fernández de la Pradilla, E. Junquera, E. Aicart, M.L. López-Rodríguez, S. Ortega-Gutiérrez, Development of molecular probes for the human 5-HT(6) receptor, J. Med. Chem. 53 (2010) 7095–7106.

[26] D. Alonso, H. Vázquez-Villa, A.M. Gamo, M.F. Martínez-Esperón, M. Tortosa, A. Viso, R. Fernández de la Pradilla, E. Junquera, E. Aicart, M. Martín-Fontecha, B. Benhamú, M.L. López-Rodríguez, S. Ortega-Gutiérrez, Development of fluorescent ligands for the human 5-HT1A receptor, ACS Med Chem Lett 1 (2010) 249–253.

[27] X. Ma, L. Shi, B. Zhang, L. Liu, Y. Fu, X. Zhang, Recent advances in bioprobes and biolabels based on cyanine dyes, Anal. Bioanal. Chem. 414 (2022) 4551–4573.

[28] J.H. Lee, H.B. Bang, S.Y. Han, J.-G. Jun, An efficient synthesis of (+)-decursinol from umbelliferone, Tetrahedron Lett. 48 (2007) 2889–2892.

[29] S. Kim, H. Ko, S. Son, K.J. Shin, D.J. Kim, Enantioselective syntheses of (+)-decursinol and (+)-trans-decursidinol, Tetrahedron Lett. 42 (2001) 7641–7643.

[30] A.M. Gamo, J.A. González-Vera, A. Rueda-Zubiaurre, D. Alonso, H. Vázquez-Villa, L. Martín-Couce, Ó. Palomares, J.A. López, M. Martín-Fontecha, B. Benhamú, M. L. López-Rodríguez, S. Ortega-Gutiérrez, Chemoproteomic approach to explore the target profile of GPCR ligands: application to 5-HT1A and 5-HT6 receptors, Chemistry 22 (2016) 1313–1321.

[31] C. Le Sueur, H.M. Hammarén, S. Sridharan, M.M. Savitski, Thermal proteome profiling: Insights into protein modifications, associations, and functions, Curr. Opin. Chem. Biol. 71 (2022), 102225.

[32] Park, B. J.; Song, G. Y.; O, Y. S.; Lee, J. H.; Yun, E. J. Pharmaceutical composition for preventing or treating aging-related diseases containing decursin derivative as active ingredient. *WO/2018/199633, PCT/KR2018/004812* **2018**.

[33] M.O. Bergo, B. Gavino, J. Ross, W.K. Schmidt, C. Hong, L.V. Kendall, A. Mohr, M. Meta, H. Genant, Y. Jiang, E.R. Wisner, N. Van Bruggen, R.A. Carano, S. Michaelis, S.M. Griffey, S.G. Young, Zmpste24 deficiency in mice causes spontaneous bone fractures, muscle weakness, and a prelamin A processing defect, Proc. Natl. Acad. Sci. USA 99 (2002) 13049–13054.

[34] A.M. Pendás, Z. Zhou, J. Cadiñanos, J.M. Freije, J. Wang, K. Hultenby, A. Astudillo, A. Wernerson, F. Rodríguez, K. Tryggvason, C. López-Otín, Defective prelamin A processing and muscular and adipocyte alterations in Zmpste24 metalloproteinase-deficient mice, Nat. Genet. 31 (2002) 94–99.

[35] R. Varga, M. Eriksson, M.R. Erdos, M. Olive, I. Harten, F. Kolodgie, B.C. Capell, J. Cheng, D. Faddah, S. Perkins, H. Avallone, H. San, X. Qu, S. Ganesh, L.B. Gordon, R. Virmani, T.N. Wight, E.G. Nabel, F.S. Collins, Progressive vascular smooth muscle cell defects in a mouse model of Hutchinson-Gilford progeria syndrome, Proc. Natl. Acad. Sci. USA 103 (2006) 3250–3255.

[36] F.G. Osorio, C.L. Navarro, J. Cadinanos, I.C. Lopez-Mejia, P.M. Quiros, C. Bartoli, J. Rivera, J. Tazi, G. Guzman, I. Varela, D. Depetris, F. de Carlos, J. Cobo, V. Andres, A. De Sandre-Giovannoli, J.M. Freije, N. Levy, C. Lopez-Otin, Splicing-directed therapy in a new mouse model of human accelerated aging, Sci. Transl. Med. 3 (2011) 106ra107.

[37] B. Schmidt, F. Wolf, C. Ehlert, Systematic investigation into the Matsuda-Heck reaction of α-methylene lactones: how conformational constraints direct the β-H-elimination step, J. Org. Chem. 81 (2016) 11235–11249.
[38] J.-H. Lee, H.-B. Bang, S.Y. Han, J.-G. Jun, A convenient total synthesis of (+)-decursinol from resorcinol, Bull. Korean Chem. Soc. 27 (2006) 2104–2106.
[39] D.G. McCafferty, J.A. Pollock, D.M. Gooden, M.G. Caron, R.R. Gainetdinov, T.D. Sotnikova, Methods of treatment using arylcyclopropylamine compounds. *Patent US20130178520A1* **2013**.